

Article

Heat Transport Phenomena for the Darcy–Forchheimer Flow of Casson Fluid over Stretching Sheets with Electro-Osmosis Forces and Newtonian Heating

Xianqin Zhang ¹, Dezhi Yang ², Muhammad Israr Ur Rehman ³ and Aamir Hamid ^{4,*}¹ College of Management, Qingdao University of Technology, Linyi 273400, China; zhangxianqin@qut.edu.cn² College of Science, Qingdao University of Technology, Linyi 273400, China; dezhiyangqdlg@163.com³ School of Mathematics and Statistics, Central South University, Changsha 410083, China; ibrarg1708@gmail.com⁴ Fluids Group, Faculty of Mechanical Engineering, Istanbul Technical University, Istanbul 34437, Turkey

* Correspondence: aamirhameed@math.qau.edu.pk

Abstract: In this study, an investigation has been carried out to analyze the impact of electro-osmotic effects on the Darcy–Forchheimer flow of Casson nanofluid past a stretching sheet. The energy equation was modelled with the inclusion of electro-osmotic effects with viscous and Joule dissipations. The governing system of partial differential equations were transformed by using the suitable similarity transformations to a system of ordinary differential equations and then numerically solved by using the Runge–Kutta–Fehlberg method with a shooting scheme. The effects of various parameters of interest on dimensionless velocity and temperature distributions, as well as skin friction and heat transfer coefficient, have been adequately delineated via graphs and tables. A comparison with previous published results was performed, and good agreement was found. The results suggested that the electric and Forchheimer parameters have the tendency to enhance the fluid velocity as well as momentum boundary layer thickness. Enhancements in temperature distribution were observed for growing values of Eckert number. It was also observed that higher values of electric field parameter diminished the wall shear stress and local Nusselt number.

Keywords: Darcy–Forchheimer porous medium; electro-osmosis forces (EOFs); MHD; Ohmic heating; Casson fluid; stretching sheet



Citation: Zhang, X.; Yang, D.; Israr Ur Rehman, M.; Hamid, A. Heat Transport Phenomena for the Darcy–Forchheimer Flow of Casson Fluid over Stretching Sheets with Electro-Osmosis Forces and Newtonian Heating. *Mathematics* **2021**, *9*, 2525. <https://doi.org/10.3390/math9192525>

Academic Editor: Efstratios Tzirtzilakis

Received: 29 August 2021

Accepted: 4 October 2021

Published: 8 October 2021

Publisher's Note: MDPI stays neutral with regard to jurisdictional claims in published maps and institutional affiliations.



Copyright: © 2021 by the authors. Licensee MDPI, Basel, Switzerland. This article is an open access article distributed under the terms and conditions of the Creative Commons Attribution (CC BY) license (<https://creativecommons.org/licenses/by/4.0/>).

1. Introduction

The flow driven by a stretchable sheet is significant because the ultimate desirable output is heavily impacted by the rate of stretchable and heat transport at the surface, representing wide applicability in industrial and manufacturing procedures. Stretching is utilized in metal extrusions and plastic, the development of thin sheets or polymer films, and the manufacture of glass fibers, to name a few applications. Filaments and polymer sheeting are made in industry by continuously extruding material from a die to a windup roller that is a fixed distance away. Throughout an ambient fluid, thin polymers which produce a continuously movable surface with a non-uniform velocity were investigated by Takhar [1]. The flow of Casson liquid in a pipe was explored by Fredrickson [2]. Mukhopadhyay [3] discussed the effect of heat radiation on the unsteady flow of Casson liquid generated by a stretched sheet exposed to blowing/suction. The closed-form solution for steady 2D and incompressible viscous liquid flow produced by stretch was presented by Crane [4]. The 3D hydromagnetic flow of Casson liquid in permeable media was also observed by Nadeem et al. [5]. Mustafa et al. [6] inspected the heat transport and flow of the boundary layer of a Casson fluid along a movable flat plate with a paralleled free stream and addressed the question analytically, utilizing the homotopy analysis method. Ibrahim and Makinde [7] reported the numerical outcomes of electrically showing the slip flow of Casson

nanofluid produced while a stretching sheet was under the effect of convective boundary condition utilizing similarity alterations. The boundary layer Casson liquid flow for exact solutions across a porous stretch/shrink sheet with and without an externally applied Hartman force was described by Bhattacharyya et al. [8,9]. Oyelakin et al. [10] determined unsteady Casson nanofluid movement electrically, showing the absence of convective boundary and slip conditions. Recently, Sajid et al. [11] investigated the combined effects of viscous dissipation and chemical reactions on micropolar Prandtl fluid induced by a stretching surface. They suggested that the radiation parameter is the key factor to improve the heat transfer rate. The transient flow of Casson nanofluid over a stretching sheet was analyzed by Jamshed et al. [12] with thermal radiation and a convectively heated surface. Waqas et al. [13] discussed the impact of magnetic parameters on Carreau–Yasuda nanofluid along a stretching sheet in the presence of motile microorganisms. Their study showed that drag force decreased the motion of the fluid. Articles [14–20] discuss the significant properties of heat transport and fluid flow of numerous non-Newtonian liquids towards a stretchable/shrinkable sheet.

In several fields of industry and engineering, the effects of chemical reactions and MHD in heat and mass transport flow are significant. This represents significant impacts in MHD pumps, augmented oil recovery, the importance of ceramic jets and cooling's towers, etc., under the impact of Hartman field; Takhar et al. [21] investigated the chemical reactions and influence on boundary layer movement across a stretchable sheet. They discovered that a Hartman field greatly increased skin friction. Pavlov [22] examined whether an externally applied Hartman field affected MHD flow across a stretchable sheet. The dissipation flow of an MHD nanoparticle through an elongating surface was depicted by Imtiaz et al. [23]. When the Hartman field was enhanced, the flow of non-dimensional liquid was reduced. The MHD flow for multiple solutions of Casson fluid across a perpendicular stretchable sheet with radiation and slip velocity were considered by Ramudu et al. [24]. The 2D electrically conducting nanofluid flow over a stretchable sheet under the influence of convective surface condition was examined by Khan et al. [25]. Anderson [26] analyzed the impact of transverse magnetic field on viscoelastic fluid induced by a stretching surface. Mukhopadhyay et al. [27] discussed the 2D and incompressible flow of electrically conducting fluid along a heated stretching surface in the presence of variable viscosity. In the absence and existence of a Hartman field, the impact of a first-order chemical process on 2D viscous fluid flow was observed by Mohyud-Din et al. [28] and Khan et al. [29]. The pattern of solute dispersion in the flow of an MHD boundary layer across a stretched sheet was described by Bhattacharyya and Layek [30]. Hayat et al. [31] analytically studied the impact of mixed convection flow of power-law fluid over a wedge-shaped geometry. Moreover, several important features of MHD flow across a stretchable sheet have been analyzed in numerous articles [32–35] in the literature.

In recent decades, electro-osmosis has been observed to a large extent. The movement of an electrolyte via a conduit with a voltage charge barrier is known as electro-osmosis. Fluid dialysis, porous membranes, zoological processes, transportation through human skin, tube/canal flow, and separation techniques are all examples of electro-osmosis in biological, clinical, and manufacturing systems. For instance, Misra and Sinha [36] examined the heat transport mechanisms of the electro-osmosis flow of non-Newtonian fluid in a microchannel. Nagler [37] investigated the combined effects of MHD and electro-osmosis on Jaffery–Hamel flow inside a wedge channel in the presence of nanoparticles. Later, El-dabe et al. [38] analytically studied the impact of Hall current on the peristaltic flow of nanofluid in the presence of electro-osmotic forces. The influence of slip mechanisms on magneto Oldroyd-B fluid past a parallel plate microchannel in the presence of electro-osmosis forces was investigated by Wang et al. [39]. Yang et al. [40] optimized the entropy generation of electro-osmotic flow of third-grade fluid past a microchannel. Furthermore, Sira et al. [41] obtained an exact solution of electro-osmotic flow of magnetized non-Newtonian fluid over a rotating microchannel. Zaher et al. [42] analyzed the electro-osmotic forces in the non-Darcian flow of Williamson fluid containing microorganisms. Moreover, Rajaram

et al. [43] discussed the effects of thermal radiation on the electro-osmotic flow of Casson fluid towards an exponentially stretching sheet.

To the best of the authors’ knowledge, this field has never been investigated in scientific research. The main aim of this study was to analyze the flow and heat transport mechanisms of the Darcy–Forchheimer flow of non-Newtonian Casson fluid along a stretching sheet. Furthermore, the impact of electro-osmosis forces, viscous dissipation and Newtonian heating on Casson fluid were investigated in this study. The governing partial differential equations were modified and converted to nonlinear ordinary differential equations and then numerically tackled by shooting [44–47]. The impacts of embedded flow control parameters on fluid velocity, temperature, velocity gradient, and heat transfer rate have been graphically demonstrated and explored. Comparisons of numerical results were performed against the previously published data under limited cases and observed to be in good agreement.

2. Mathematical Formulation

This study explored the steady, incompressible 2D MHD flow of non-Newtonian Casson fluid towards a stretchable sheet with the presence of electro-osmotic forces. The surface was stretched at $u_w = ax$ ($a > 0$) and heated utilizing Newtonian heating. The x – axis was parallel to the stretchable surface and y – axis was normal to it (as shown in Figure 1). The governing boundary layer equation under the liquid flow and boundary layer assumption are presented in Figure 1.

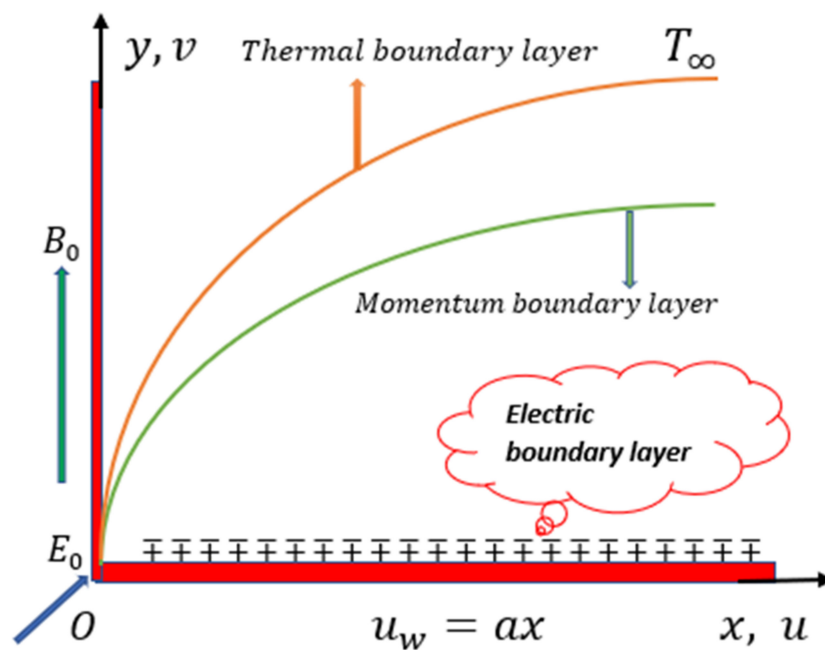


Figure 1. Pertinent sketch of the boundary layer problem.

$$\frac{\partial u}{\partial x} + \frac{\partial v}{\partial y} = 0 \tag{1}$$

$$u \frac{\partial u}{\partial x} + v \frac{\partial u}{\partial y} = v \left(1 + \frac{1}{\beta} \right) \frac{\partial^2 u}{\partial y^2} + \sigma (E_0 B_0 - B_0^2 u) - \frac{\mu}{k} u - \frac{F}{\sqrt{k}} u^2 \tag{2}$$

$$u \frac{\partial T}{\partial x} + v \frac{\partial T}{\partial y} = \frac{K}{\rho C_p} \frac{\partial^2 T}{\partial y^2} + \sigma (E_0 B_0 - B_0^2 u)^2 + \frac{\mu}{\rho C_p} \left(1 + \frac{1}{\beta} \right) \left(\frac{\partial u}{\partial y} \right)^2 \tag{3}$$

where the velocity component (u, v) is oriented in the (x, y) direction. $\nu, C_p, \sigma, K, T, \beta, \mu$ and ρ are the kinematic viscosity, specific heat, electric conductivity, thermal conductivity,

fluid temperature, Casson fluid, dynamic viscosity, and density, respectively. The flow is constrained by the following boundary conditions:

$$\begin{aligned}
 u = u_w, v = 0, \frac{\partial T}{\partial y} = -h_s T(NH), \text{ at } y = 0, \\
 u \rightarrow 0, T \rightarrow T_\infty, \text{ as } y \rightarrow \infty,
 \end{aligned}
 \tag{4}$$

For non-Newtonian heating, h_s is the heat transmission parameter utilizing the transmission above:

$$\eta = y\sqrt{\frac{a}{v}}, \psi(x, y) = \sqrt{av}xf(\eta), \theta(\eta) = \frac{T - T_\infty}{T_\infty}
 \tag{5}$$

where ψ is determined in the conventional way, i.e., $v = -\frac{\partial \psi}{\partial x}$, $u = \frac{\partial \psi}{\partial y}$, and (η) is the similarity factor. Equation (1) is fulfilled immediately, and Equations (2)–(4) are simplified to:

$$\left(1 + \frac{1}{\beta}\right)f'' - (1 + F_s)(f')^2 + ff'' + M(E_1 - f') - \left(\frac{1}{Re_x}\right)\left(\frac{1}{Da}\right)f' = 0
 \tag{6}$$

$$\theta'' + EcPr\left(1 + \frac{1}{\beta}\right)(f')^2 + Prf\theta' + MEc(f' - E_1)^2 = 0
 \tag{7}$$

The subjected boundary conditions are:

$$\begin{aligned}
 f(\eta) = 0, f'(\eta) = 1, \theta'(\eta) = -\gamma[1 + \theta(\eta)], \text{ at } \eta = 0 \\
 f'(\eta) \rightarrow 0, \theta(\eta) \rightarrow 0, \text{ at } \eta \rightarrow \infty
 \end{aligned}
 \tag{8}$$

In the above equation, $\beta, \gamma, Pr, Re_x, Da, M, E_1, F_s$ and Ec represent the Casson parameter, non-Newtonian heating parameter, Prandtl number, Reynold number, Hartman number, electric field parameter, Forchheimer number and Eckert number, respectively. These parameters are defined as follows:

$$\begin{aligned}
 \gamma = h_s\sqrt{\frac{v}{a}}, Pr = \frac{v}{\alpha}, Re_x = \frac{u_w(x)x}{v}, M = \frac{\sigma B_0^2}{\rho a}, \\
 E_1 = \frac{E_0}{axB_0}, F_s = \frac{F}{\sqrt{k}}x, Ec = \frac{u_w^2}{C_p T_\infty}
 \end{aligned}
 \tag{9}$$

The pertinent variables of involvement are the co-efficient of skin friction, C_{fx} , and the Nusselt number, Nu_x , which are expressed as:

$$\begin{aligned}
 C_{fx} = \frac{\left[\left(1 + \frac{1}{\beta}\right)\frac{\partial u}{\partial y}\right]_{y=0}}{\rho u_w^2}, Nu_x = \frac{x\left(\frac{\partial T}{\partial y}\right)_{y=0}}{T_\infty}, \\
 Re_x^{\frac{1}{2}}C_{fx} = \left(1 + \frac{1}{\beta}\right)f'(0), Re_x^{-\frac{1}{2}}Nu_x = -\theta'(0)
 \end{aligned}
 \tag{10}$$

where $Re_x = \frac{u_w}{v_f}x$ is the local Reynold number.

3. Solution Methodology

The outcomes of the mathematical model illustrated in Equations (6)–(8) were obtained by employing an efficient numerical technique known as the Runge–Kutta–Fehlberg method along with the shooting scheme. Below mentioned procedures were invoked for the solutions:

$$f = Y_1, f' = Y_2, f'' = Y_3, \theta = Y_4, \theta' = Y_5,
 \tag{11}$$

$$\begin{pmatrix} Y_1' \\ Y_2' \\ Y_3' \\ Y_4' \\ Y_5' \end{pmatrix} = \begin{pmatrix} Y_2 \\ Y_3 \\ \frac{-[Y_1 Y_3 - (1 - F_s)Y_2^2 + M(E_1 - Y_2) - \frac{1}{Re_x} \frac{1}{Da} Y_2]}{\left(1 + \frac{1}{\beta}\right)} \\ Y_5 \\ -[EcPr\left(1 + \frac{1}{\beta}\right)Y_3^2 + PrY_1 Y_5 + MEc(Y_2 - E_1)] \end{pmatrix}
 \tag{12}$$

With initial condition:

$$\begin{pmatrix} Y_1(0) \\ Y_2(0) \\ Y_2(\infty) \\ Y_4(0) \\ Y_4(\infty) \end{pmatrix} = \begin{pmatrix} 0 \\ 1 \\ 0 \\ \gamma(1 + Y_0(4)) \\ 0 \end{pmatrix} \tag{13}$$

4. Results and Discussion

The numerical approach presented above was used for numerous pertinent parameter values, including the Casson parameter (β), electric parameter (E_1), Hartman number (M), Forchheimer number (F_s), Ecker number (Ec), Reynold number (Re_x), non-Newtonian heating parameter (γ) and permeability parameter (D_a) to derive the impacts of those variable on dimensionless velocity and temperature gradients. The computed outcomes are visualized in Figures 2–6, with the differences in velocity and temperature presented.

Figure 2a illustrates that as the (β) is enhanced, the velocity curve $f'(\eta)$ and the thickness of the momentum boundary reduce. Figure 2b illustrates the impact of the Hartman number (M) on the velocity curve $f'(\eta)$. It was discovered that enhancing (M) reduced the thickness of the momentum boundary layer and velocity estimation $f'(\eta)$. This is because an increment in (M) causes the Lorentz force to enhance, which restricts the flow. Figure 3a,b depicts that increasing (E_1) and (F_s) raises the thickness of the momentum boundary layer and the velocity estimation $f'(\eta)$. The large values of (Re_x) and (D_a) enhance the boundary layer velocity, as displayed in Figure 4a,b, whereas an increase in (Re_x) coincides with a decrease in viscosity, and the flow velocity grows. This is because greater values of (D_a) decrease porosity, which causes the drag coefficient to decay, and hence, the velocity to be improved.

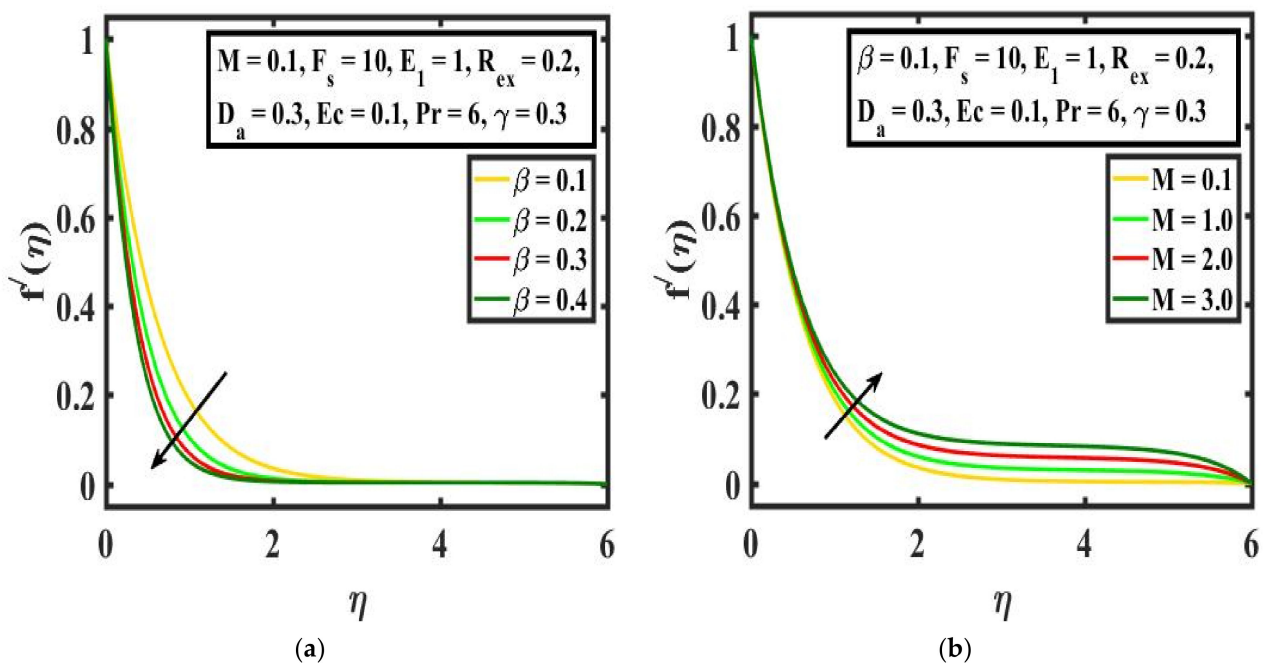


Figure 2. (a,b) The effect of $f'(\eta)$ for several values of β and M .

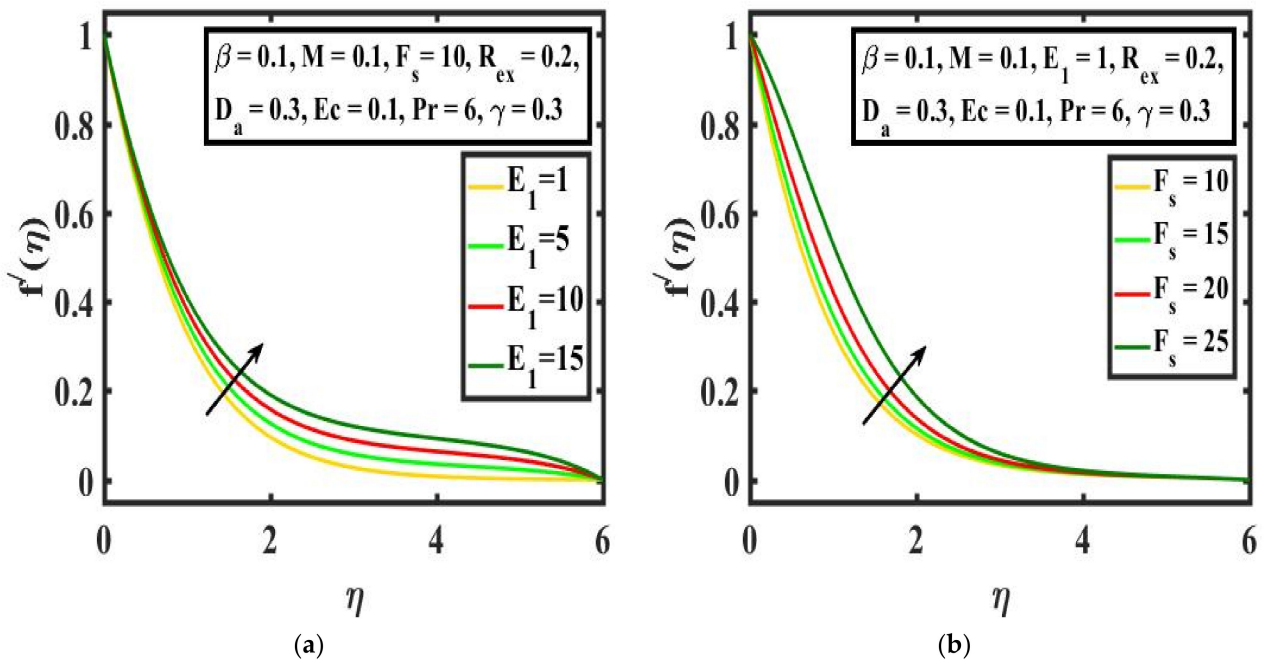


Figure 3. (a,b) The effect of $f'(\eta)$ for several values of E_1 and F_s .

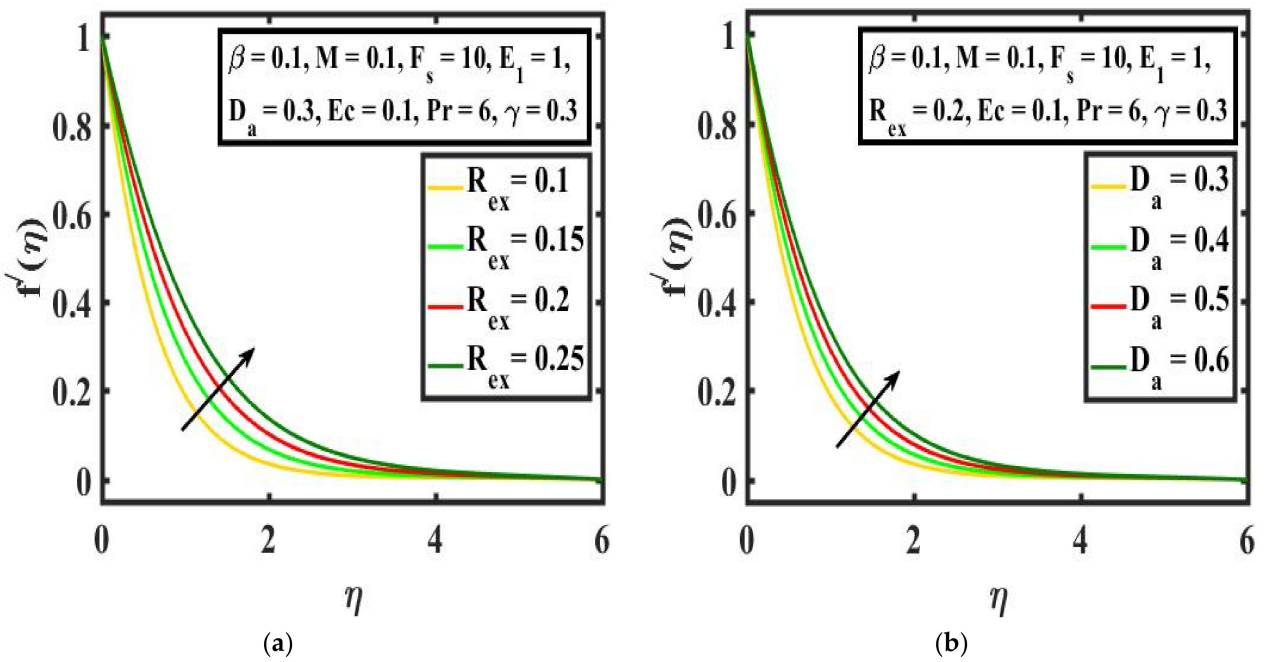


Figure 4. (a,b) The impact of $f'(\eta)$ for several values of R_{ex} and D_a .

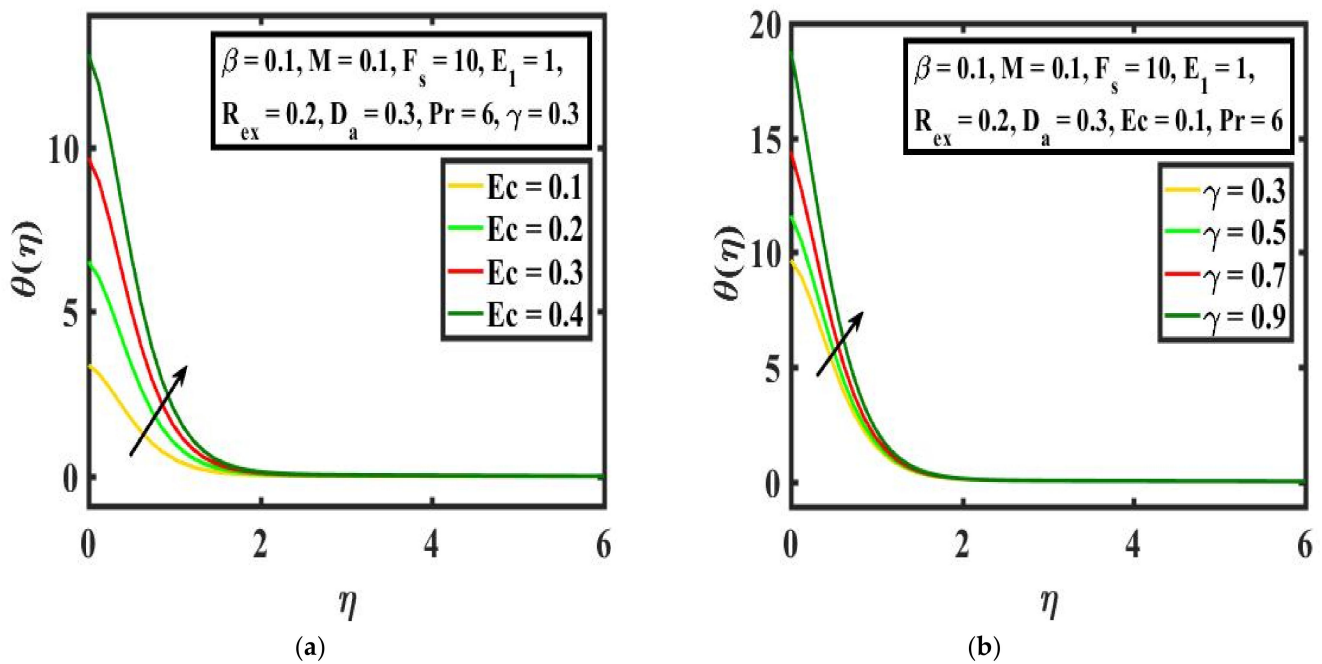


Figure 5. (a,b) The influence of $\theta(\eta)$ for numerous values of Ec and γ .

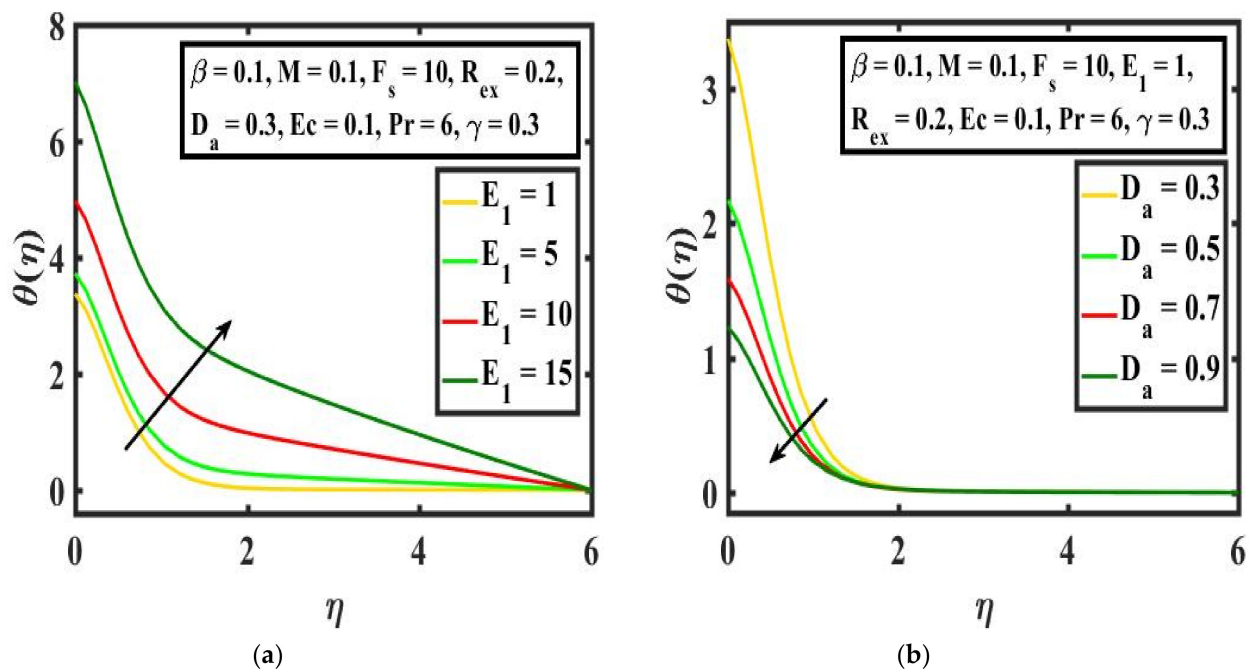


Figure 6. (a,b) The effect of $\theta(\eta)$ for numerous values of E_1 and D_a .

Figure 5a depicts the temperature estimation, $\theta(\eta)$, for a numerous value of (Ec). It can be observed that increasing the (Ec) leads to enhancements in the surface temperature. Moreover, at a larger (Ec), the thickness of thermal boundary layer is observed to be thicker. The influence of (γ) across the heat transport is depicted in Figure 5b. It can be observed that as the (γ) grows, the rate of heat transport also enhances on the surface. Figure 6a illustrates that (E_1), the heat transport, decays, and similar impacts are observed when (D_a) is enhanced, which is illustrated in Figure 6b.

5. Numerical Outcomes

Tables 1 and 2 present the modifications of skin friction, $f''(0)$, and Nusselt number, $-\theta'(0)$, for several values of (β) , (M) , (E_1) , (D_a) , (Ec) and (γ) . The numerical values of skin friction $f''(0)$ reduce with an enhanced electric field parameter, (E_1) , permeability parameter, (D_a) , and Casson parameter, (β) ; furthermore, $f''(0)$ is enhanced for increased values of the Hartman number (M) . The numerical outcomes of the Nusselt number, $-\theta'(0)$, grow with increases in (Ec) and (γ) , and exhibit contrasting behavior for increasing values of (E_1) and (D_a) . A comparison of the local Nusselt number, $-\theta'(0)$, for varying values of Prandtl number with earlier studies by Khan and Pop [48] and Alsaedi et al. [49] was performed to confirm our numerical technique. Table 3 shows that these studies have a high level of agreement.

Table 1. $f''(0)$ for $F_s = 10, Ec = 0.1, Pr = 6, R_{ex} = 0.2$ and $\gamma = 0.3$.

β	M	E_1	D_a	$f''(0)$
0.1	0.1	0.1	2	6.1508
0.2				6.1457
0.3				6.1454
0.4				6.1453
	0.2			6.2304
	0.3			6.3101
	0.4			6.3897
		0.3		6.1107
		0.5		6.0706
		0.7		6.0307
			2.1	5.9135
			2.2	5.6978
			2.3	5.5009

Table 2. $-\theta'(0)$ for $\beta = 0.1, M = 0.1, Pr = 6, R_{ex} = 0.2$ and $F_s = 10$.

Ec	γ	E_1	D_a	$-\theta'(0)$
0.1	0.3	0.1	2	0.51881
0.2				0.67938
0.3				0.83994
0.4				1.0005
	0.5			0.99323
	0.7			1.6334
	0.9			2.5444
		0.3		0.51643
		0.5		0.51431
		0.7		0.51244
			2.1	0.5156
			2.2	0.51268
			2.3	0.51001

Table 3. Comparison table of numerical results for the Nusselt number, $-\theta'(0)$, for different values of Pr .

Pr	Khan and Pop [48]	Alsaedi et al. [49]	Present Study
0.05	0.05996251	0.05996250	0.05996253
0.50	0.40391254	0.40391252	0.40391253
3.0	1.10010012	1.10010010	1.10010012
10.0	2.00152652	2.00152651	2.00152654

6. Concluding Remarks

In this study, the effects of electro-osmosis forces and magnetic field on Casson fluid flow over a stretching sheet in the presence of viscous dissipation, Ohmic heating and a Darcy–Forchheimer porous medium were investigated. The system of governing equations has been converted to dimensionless differential equations by employing similarity transformations; then, the shooting technique was implemented to derive numerical solutions and the relevant data for wall shear stress and heat flux. The impact of various physical parameters such as the porosity factor, electric field parameter, Casson fluid parameter, and Prandtl and Eckert numbers on flow profiles are discussed in detail. In light of the present investigation, we found that the electric field parameter enhanced the velocity and temperature of the Casson fluid. It was observed that Forchheimer parameter enhanced the fluid velocity, and a reverse trend was seen for the Casson fluid parameter. Furthermore, the temperature distribution was enhanced with an increase in electric field and decreased with the permeability parameter. The skin friction coefficient and the heat transfer rate were diminished by augmenting the values of the permeability parameter. Moreover, the rate of heat transfer was augmented with a higher Eckert number, whereas the reverse behavior was observed for the electric field parameter.

Author Contributions: Conceptualization, A.H.; Writing—original draft preparation, M.I.U.R.; Supervision, D.Y.; Methodology, X.Z. All authors have read and agreed to the published version of the manuscript.

Funding: This research received no external funding.

Institutional Review Board Statement: Not applicable.

Informed Consent Statement: Not applicable.

Data Availability Statement: Not applicable.

Conflicts of Interest: The authors declare no conflict of interest.

Nomenclature

u, v	Velocity components (m/s)	Pr	Prandtl number
x, y	Cartesian coordinates (m)	C_f	Skin friction coefficient
Ec	Eckert number	F_s	Forchheimer number
β	Non-Newtonian Casson fluid	k	Permeability of porous space
T_∞	Ambient temperature (K)	Nu	Local Nusselt number
E_1	Electric parameter	η	Dimensionless similarity variable
u_w	Stretching velocity	ρ	Fluid density (kg/m ³)
D_a	Permeability parameter	μ	Generalized Newtonian viscosity (Pa·s)
c_p	Specific heat	R_{ex}	Local Reynolds number
v_w	Mass flux velocity (m/s)	K	Thermal conductivity (W/m K)
F	Non-uniform inertia factor	γ	Chemical reaction
B_0	Magnetic parameter (kg/A s ²) Tesla	ν	Kinematic viscosity (m ² /s)
T	Fluid temperature (K)	ψ	Stream function
θ	Dimensionless temperature	a	Constants (m)

References

1. Takhar, H.S.; Chamka, A.J.; Nath, G. Unsteady three-dimensional MHD-boundary-layer flow due to the impulsive motion of a stretching surface. *Acta Mech.* **2001**, *146*, 59. [\[CrossRef\]](#)
2. Fredrickson, A.G. *Principles and Applications of Rheology*; Prentice-Hall: Englewood Cliffs, NJ, USA, 1964.
3. Mukhopadhyay, S. Effects of thermal radiation on Casson fluid flow and heat transfer over an unsteady stretching surface subjected to suction/blowing. *Chin. Phys. B* **2013**, *22*, 114702. [\[CrossRef\]](#)
4. Crane, L.J. Flow past a stretching plate. *J. Appl. Math. Phys.* **1970**, *21*, 645. [\[CrossRef\]](#)
5. Nadeem, S.; Haq, R.U.; Akbar, N.S.; Khan, Z.H. MHD three-dimensional Casson fluid flow past a porous linearly stretching sheet. *Alex. Eng. J. Fac. Eng. Alex. Univ.* **2013**, *52*, 577–582. [\[CrossRef\]](#)

6. Mustafa, M.; Hayat, T.; Pop, I.; Aziz, A. Unsteady boundary layer flow of a Casson fluid due to an impulsively started moving flat plate. *Heat Transfer*. **2011**, *40*, 563–576. [[CrossRef](#)]
7. Ibrahim, W.; Makinde, O.D. Magnetohydrodynamic stagnation point flow and heat transfer of Casson nanofluid past a stretching sheet with slip and convective boundary condition. *J. Aerosp. Eng.* **2015**, *29*, 04015037. [[CrossRef](#)]
8. Bhattacharyya, K.; Hayat, T.; Alsaedi, A. Exact solution for boundary layer flow of Casson fluid over a permeable stretching/shrinking sheet. *Z. für Angew. Math. und Mech.* **2013**, *94*, 522–528. [[CrossRef](#)]
9. Bhattacharyya, K.; Hayat, T.; Alsaedi, A. Analytic solution for magnetohydrodynamic boundary layer flow of Casson fluid over a stretching/shrinking sheet with wall mass transfer. *Chin. Phys. B* **2013**, *22*, 024702. [[CrossRef](#)]
10. Oyelakin, I.S.; Mondal, S.; Sibanda, P. Unsteady Casson nanofluid flow over a stretching sheet with thermal radiation, convective and slip boundary conditions. *Alex. Eng. J. Fac. Eng. Alex. Univ.* **2016**, *55*, 1025–1035. [[CrossRef](#)]
11. Sajid, T.; Jamshed, W.; Shahzad, F.; Eid, M.R.; Alshehri, H.M.; Goodarzi, M.; Akgül, E.K.; Nisar, K.S. Micropolar fluid past a convectively heated surface embedded with n th order chemical reaction and heat source/sink. *Phys. Scr.* **2021**, *96*, 104010. [[CrossRef](#)]
12. Jamshed, W.; Devi, S.U.; Goodarzi, S.M.; Prakash, M.; Nisar, K.S.; Zakarya, M.; Abdel-Aty, A.-H. Evaluating the unsteady Casson nanofluid over a stretching sheet with solar thermal radiation: An optimal case study. *Case Stud. Therm. Eng.* **2021**, *26*, 101160. [[CrossRef](#)]
13. Waqas, H.; Farooq, U.; Khan, S.A.; Alshehri, H.M.; Goodarzi, M. Numerical analysis of dual variable of conductivity in bioconvection flow of Carreau–Yasuda nanofluid containing gyrotactic motile microorganisms over a porous medium. *J. Therm. Anal. Calorim.* **2021**, *145*, 2033–2044. [[CrossRef](#)]
14. Abdelsalam, S.I.; Mekheimer, K.S.; Zaher, A.Z. Alterations in blood stream by electroosmotic forces of hybrid nanofluid through diseased artery: Aneurysmal/stenosed segment. *Chin. J. Phys.* **2020**, *65*, 123–138. [[CrossRef](#)]
15. Akolade, M.T.; Adeosun, T.; Olabode, J. Influence of thermophysical features on MHD squeezed flow of dissipative Casson fluid with chemical and radiative effects. *J. Appl. Comput. Mech.* **2020**, *2021*, 1–11.
16. Mekheimer, K.S.; Zaher, A.Z.; Hasona, W.M. Entropy of ac electro-kinetics for blood mediated gold or copper nanoparticles as a drug agent for thermotherapy of oncology. *Chin. J. Phys.* **2020**, *65*, 123–138. [[CrossRef](#)]
17. Nagaraja, B.; Gireesha, B.J. Exponential space-dependent heat generation impact on MHD convective flow of Casson fluid over a curved stretching sheet with chemical reaction. *J. Therm. Anal. Calorim.* **2021**, *143*, 4071–4079. [[CrossRef](#)]
18. Hussain, M.; Ali, A.; Ghaffar, A.; Inc, M. Flow and thermal study of MHD Casson fluid past a moving stretching porous wedge. *J. Therm. Anal. Calorim.* **2021**, *102*, 1–11.
19. Ramudu, A.V.; Kumar, K.A.; Sugunamma, V.; Sandeep, N. Impact of Soret and Dufour on MHD Casson fluid flow past a stretching surface with convective–diffusive conditions. *J. Therm. Anal. Calorim.* **2021**, *182*, 1–11.
20. Hussain, M.; Ghaffar, A.; Ali, A.; Shahzad, A.; Nisar, K.S.; Alharthi, M.R.; Jamshed, W. MHD thermal boundary layer flow of a Casson fluid over a penetrable stretching wedge in the existence of nonlinear radiation and convective boundary condition. *Alex. Eng. J.* **2021**, *60*, 5473–5483. [[CrossRef](#)]
21. Takhar, H.S.; Chamkha, A.J.; Nath, G. Flow and mass transfer on a stretching sheet with a magnetic field and chemically reactive species. *Int. J. Eng. Sci.* **2000**, *38*, 1303–1314. [[CrossRef](#)]
22. Pavlov, K.B. Magnetohydrodynamic flow of an incompressible viscous fluid caused by the deformation of a plane surface. *Magnetohydrodynamics* **1974**, *10*, 146–148.
23. Imtiaz, M.; Hayat, T.; Alsaedi, A. Flow of magneto nanofluid by a radiative exponentially stretching surface with dissipation effect. *Adv. Powder Technol.* **2016**, *27*, 2214–2222. [[CrossRef](#)]
24. Venkata Ramudu, A.C.; Anantha Kumar, K.; Sugunamma, V.; Sandeep, N. Influence of suction/injection on MHD Casson fluid flow over a vertical stretching surface. *J. Therm Anal. Calorim.* **2019**, *113*, 3675–3682. [[CrossRef](#)]
25. Khan, W.A.; Makinde, O.D.; Khan, Z.H. Non-aligned MHD stagnation point flow of variable viscosity nanofluids past a stretching sheet with radiative heat. *Int. J. Heat Mass Transf.* **2016**, *96*, 525–534. [[CrossRef](#)]
26. Andersson, H.I. MHD flow of a viscoelastic fluid past a stretching surface. *Acta Mech.* **1992**, *95*, 227–230. [[CrossRef](#)]
27. Mukhopadhyay, S.; Layek, G.C.; Samad, S.A. Study of MHD boundary layer flow over a heated stretching sheet with variable viscosity. *Int. J. Heat Mass Transf.* **2005**, *48*, 4460–4466. [[CrossRef](#)]
28. Mohyud-Din, S.T.; Ahmed, N.; Khan, U.; Waheed, A.; Hussain, S.; Darus, M. On Combined Effects of Heat Transfer and Chemical Reaction for the Flow through an Asymmetric Channel with Orthogonally Deformable Porous Walls. *Math. Probl. Eng.* **2016**, *2016*, 2568785. [[CrossRef](#)]
29. Khan, U.; Ahmed, N.; Mohyud-Din, S.T. Thermo-diffusion, diffusion-thermo and chemical reaction effects on MHD flow of viscous fluid in divergent and convergent channels. *Chem. Eng. Sci. Elsevier* **2016**, *141*, 17–27. [[CrossRef](#)]
30. Bhattacharyya, K.; Layek, G.C. Chemically reactive solute distribution in MHD boundary layer flow over a permeable stretching sheet with suction or blowing. *Chem. Eng. Commun.* **2010**, *197*, 1527–1540. [[CrossRef](#)]
31. Hayat, T.; Hussain, M.; Nadeem, S.; Mesloub, S. Falkner-Skan wedge flow of a power-law fluid with mixed convection and porous medium. *Comput. Fluids* **2011**, *49*, 22–28. [[CrossRef](#)]
32. Gireesha, B.J.; Shankaralingappa, B.M.; Prasannakumar, B.C.; Nagaraja, B. MHD flow and melting heat transfer of dusty Casson fluid over a stretching sheet with Cattaneo–Christov heat flux model. *Int. J. Ambient Energy* **2020**, *41*, 1–9. [[CrossRef](#)]

33. Hussain, A.; Sana, A.; Rizwana, R.; Malik, M.Y. MHD stagnation point flow of a Casson fluid with variable viscosity flowing past an extending/shrinking sheet with slip effects. *Phys. A Stat. Mech. Its Appl.* **2020**, *553*, 124080. [[CrossRef](#)]
34. Hamid, A.; Khan, M. Multiple solutions for MHD transient flow of Williamson nanofluids with convective heat transport. *J. Taiwan Inst. Chem. Eng.* **2019**, *103*, 126–137.
35. Kumar, C.P. Thermal Diffusion and Inclined Magnetic Field Effects on MHD Free Convection Flow of Casson Fluid Past an Inclined Plate in Conducting Field. *Turk. J. Comput. Math. Educ. (TURCOMAT)* **2021**, *12*, 960–977.
36. Misra, J.C.; Sinha, A. Electro-osmotic flow and heat transfer of a non-Newtonian fluid in a hydrophobic microchannel with Navier slip. *J. Hydrodyn. Ser. B* **2015**, *27*, 647–657. [[CrossRef](#)]
37. Nagler, J. On the electroosmotic and MHD Jeffery–Hamel flow of Nano fluid influenced by wall slip conditions. *J. Polytech.* **2016**, *19*, 555–568.
38. El-Dabe, N.T.M.; Moatimid, G.M.; Hassan, M.A.; Godh, W.A. Electro-osmotic and Hall Current Effects on the Nanofluid Flow through Porous Medium with Wall Properties. *Int. J. Appl. Eng. Res.* **2019**, *14*, 3552–3565.
39. Wang, X.; Xu, H.; Qi, H. Transient magnetohydrodynamic flow and heat transfer of fractional Oldroyd-B fluids in a microchannel with slip boundary condition. *Phys. Fluids* **2020**, *32*, 103104. [[CrossRef](#)]
40. Yang, C.; Jian, Y.; Xie, Z.; Li, F. Electromagnetohydrodynamic Electroosmotic Flow and Entropy Generation of Third-Grade Fluids in a Parallel Microchannel. *Micromachines* **2020**, *11*, 418. [[CrossRef](#)] [[PubMed](#)]
41. Siva, T.; Jangili, S.; Kumbhakar, B. Heat transfer analysis of MHD and electroosmotic flow of non-Newtonian fluid in a rotating microfluidic channel: An exact solution. *Appl. Math. Mech.* **2021**, *42*, 1047–1062. [[CrossRef](#)]
42. Zaher, A.Z.; Ali, K.K.; Mekheimer, K.S. Electroosmosis forces EOF driven boundary layer flow for a non-Newtonian fluid with planktonic microorganism: Darcy Forchheimer model, Electroosmosis forces EOF driven boundary layer flow for a non-Newtonian fluid with planktonic microorganism: Darcy Forchheimer model. *Int. J. Numer. Methods Heat Fluid Flow* **2021**, *31*, 2534–2559.
43. Rajaram, V.; Varadharaj, B.; Jayavel, P. Impact of electroosmotic flow on a Casson fluid driven by chemical reaction and convective boundary conditions. *Heat Transf.* **2021**, *50*, 4993–5019. [[CrossRef](#)]
44. Hamid, A.; Hashim; Khan, M. Impacts of binary chemical reaction with activation energy on unsteady flow of magneto-Williamson nanofluid. *J. Mol. Liq.* **2018**, *262*, 435–442. [[CrossRef](#)]
45. Hamid, A.; Hashim; Khan, M.; Hafeez, A. Unsteady stagnation-point flow of Williamson fluid generated by stretching/shrinking sheet with Ohmic heating. *Int. J. Heat Mass Transf.* **2018**, *126*, 933–940. [[CrossRef](#)]
46. Hamid, A.; Khan, M.; Alghamdi, M. Numerical simulation for transient flow of Williamson fluid with multiple slip model in the presence of chemically reacting species. *Int. J. Numer. Methods Heat Fluid Flow* **2019**, *29*, 4445–4461. [[CrossRef](#)]
47. Hamid, A. Terrific effects of Ohmic-viscous dissipation on Casson nanofluid flow over a vertical thin needle: Buoyancy assisting & opposing. *J. Mater. Res. Technol.* **2020**, *9*, 11220–11230.
48. Khan, W.A.; Pop, I. Boundary-layer flow of a nanofluid past a stretching sheet. *Int. J. Heat Mass Tran.* **2010**, *53*, 2477–2483. [[CrossRef](#)]
49. Alsaedi, A.; Awais, M.; Hayat, T. Effects of heat generation/absorption on stagnation point ow of nanofluid over a surface with convective boundary conditions. *Comm. Non-Linear Sci. Numer. Simul.* **2012**, *17*, 4210–4223. [[CrossRef](#)]